



## Modeling Optimal Locations of Breakwaters to Mitigate Wind-Induced Waves in Bahar Al-Najaf Depression Using MIKE21

Uday Abdul Sahib M. Alturfi<sup>1\*</sup>, Abdul-Hassan K. Shukur<sup>2</sup>

<sup>1</sup> Faculty of Engineering, Department of Structures and Water Resources, University of Kufa, Najaf 0054, Iraq

<sup>2</sup> Faculty of Engineering, Department of Civil Engineering, University of Babylon, Babylon 0051, Iraq

Corresponding Author Email: [oday.alturfi@uokufa.edu.iq](mailto:oday.alturfi@uokufa.edu.iq)

Copyright: ©2024 The authors. This article is published by IIETA and is licensed under the CC BY 4.0 license (<http://creativecommons.org/licenses/by/4.0/>).

<https://doi.org/10.18280/ijsse.140123>

**Received:** 5 June 2023

**Revised:** 25 July 2023

**Accepted:** 31 July 2023

**Available online:** 29 February 2024

### Keywords:

spectral wave SW, shallowwater wave, MIKE21; breakwater, numerical analysis, Bahar Al-Najaf lake, wind waves, wave modeling, wave mitigation

### ABSTRACT

The waves produced by the wind are the most noticeable and frequently the most significant waves in the range of waves at sea. Given the limited amount of knowledge on the mathematical modelling of the wind induced wave in lake or shallow water depth, considered to this point. In this paper, a briefly look at how these waves are formed by the wind in the Bahar Al-Najaf depression, as well as some of the essential properties that arise. A numerical model based on unstructured mesh is proposed to predicate and visualize wave conditions. MIKE21 spectral model base on mass balance equation was used as a numerical tool to find the optimal location of mitigation structures to dissipation the wave energy near the neighbor structures. The amount of variation between the simulated wave heights and those calculated using an empirical equation is less than 9%. Three schemes for breakwater has been tested to find the optimal location and orientation of breakwater. The results showed that the three schemes used for the breakwater gave varying results, both depending on its location and characteristics. The first scheme gave a covering area approaching 1.19 km<sup>2</sup>, and the second scheme gave approximately 0.889 km, and third scheme gave a covering area 1.11 km<sup>2</sup>. This study showed that the wave heights at the upstream and downstream were measured after the breakwater had been constructed, and they were found to be between 0.35 and 0.7 m. This implies a decrease of around 40% to 60% in comparison to the original heights of 1.25 to 0.9 m. All of these schemes are good to a certain extent in dispersing the energy by breaking the single pattern of the wave at rates that may reach 50% of the height of the arriving wave, the first scenario was the best and most efficient in terms of energy dispersion.

## 1. INTRODUCTION

A body of water that is exposed to the atmosphere is almost never seen without waves on its surface. These waves are a result of forces operating on the fluid that try to distort it in opposition to the forces of gravity and surface tension, which work together to keep the fluid's surface level. Thus, it is impossible to overstate the significance of waves. Wave motion may affect everything that is near or in a body of water. At the seashore, this may cause sand to migrate down the coastline, resulting in erosion or storm-related damage to buildings [1].

The major approaches for studying wave propagation include field observation, physical model testing, and numerical simulation. The numerical simulation approach has quickly grown in comparison to physical model testing and field observations because of its benefits including cheap cost, flexible application, quick turnaround, independence from scale effect, and availability in a testing setting [2].

For decades, researchers have been working on numerical wave water modelling. The earliest numerical models for wave water modelling were established in the 1960s and 1970s,

although their computing capacity was restricted at the time. Throughout the 1980s and 1990s, as computers got more powerful, numerical models for wave water modelling became increasingly advanced. One of the earliest numerical models for wave water modeling was the Mild Slope Equation (MSE) model, which was developed in the 1960s. The MSE model is a linear model that is used to simulate waves in shallow water, such as nearshore areas. The model presents that water depth is much smaller than the wavelength of the waves.

In the 1970s, researchers began to develop more sophisticated numerical models for wave water modeling. The Boussinesq Equation (BE) model was one of the most significant of these models. This model is a nonlinear model that is used to simulate waves in both shallow and deep water. The model considers the effects of wave breaking and wave dispersion in its calculations.

In the 1980s and 1990s, numerical models for wave water modeling continued to evolve. Researchers began to develop models that could simulate the interaction between waves and currents, as well as the effects of sediment transport. One of the most important of these models was the SWAN (Simulating Waves Nearshore) model, which was developed

in the Netherlands in the 1990s. The SWAN model is a sophisticated numerical model that can simulate wave propagation, wave breaking, and sediment transport in coastal areas [3].

One example of a modern numerical model for wave water modeling is MIKE21SW, developed by DHI in Denmark. MIKE21SW is a three-dimensional model that can simulate wave propagation, wave breaking, and wave runup in coastal areas. The model considers how tides, currents, wind, and bathymetry affect wave behavior [4]. Many studies anterior possible to remember that used modern numerical model:

WAVEWATCH III was used by Li et al. [5] in order to provide wave prediction for the Bohai Sea of China. Bi et al. [6] used WAVEWATCH III to carry out a simulated examination of the waves that are found in the Pacific Ocean. Yang and Zhang [7] used SWAN to simulate wind wave activity in Bohai Bay from 1989 to 2008 and analyze wave probability. Ayat [8] used the MIKE21 SW model to simulate waves in the East Mediterranean and Aegean waters and analyze wave energy in the relevant waters. To comprehend the effects of man-made structures like mudflats and breakwater on shoreline changes, Noujas et al. [9] used the MIKE21 SW model to study the Indian southwest coastal waves.

This paper will demonstrate the application of numerical simulation of MIKE21-SW for calculation of the wave distribution and transmission parameters to find the optimum location of proposed breakwater (3 scheme) in the depression of Najaf Sea in Iraq region. The possibility of application would be presented through find the largest protected area covered by scheme proposed with largest efficient breakwater.

## 2. DESCRIPTION OF THE STUDY AREA

One of Iraq's historic low water bodies is the Bahr Al-Najaf depression. It was regarded as a natural lake and was situated in the southwest of the Al-Najaf city Centre. The region has a total surface area of 251 km<sup>2</sup>, and its position may be determined by the coordinates 44° 11' 34" to 44° 22' 37", and 31° 47' 11" to 32° 04' 08," respectively. It has a lake within that is about 90 km<sup>2</sup> size. Due to influx, precipitation, and seasonal weather changes, that area fluctuated between increases and decreases. The area is classified as a desert where water levels rise throughout the winter owing to increasing rainfall [10]. The research area's slope progressively steepens as it moves from the west and south-west to the north and northeast. Three major valleys, Kharr, Shoaib Al-Rahimawi, and Maleh, have a wide area and provide water to the Bahr Al-Najaf Lake. These valleys also help to replenish the groundwater in the area [11].

## 3. RESEARCH PROBLEM

According to the target area, from time to time this area is subjected to flooding as a result of the rainfall-runoff releasing into the lake from the neighboring areas (due to the low-land of the area) Figure 2. As well as the result of waves caused by high winds in this region. the strategic line transformer, and the Al-Noor village is one of the most important areas that are exposed to the risk of inundation as a result of the waves generated in the lake in addition to the high wind speed in the region. Therefore, this study is prepared to employ energy

dispersal facilities and breakwater characteristics to protect the road linking the Al-Maamal area and the city of Al-Najaf, given that this road is adjacent to the Bahr Al-Najaf region, and it is exposed to the dangers of flooding and inundation from time to time. Figure 1 shows the Digital Elevation Model for the study area. Figure 2 showing the damage caused by the high-water level as a result of the generation of waves and floods in the study area in the winter of 2013.

This study was aim to a proposal for a breakwater capable of mitigating the impact of wind waves in an area that is at risk of flooding in certain seasons as a result of wave height.

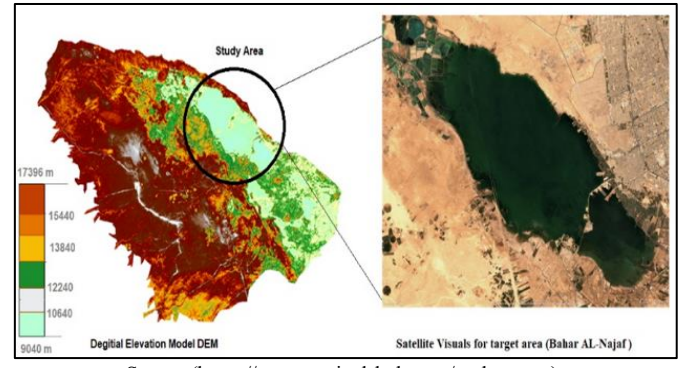


**Figure 1.** Satellite visuals of the study area shows DEM and lake border



**Figure 2.** Some pictures showing the damage caused by the high-water level as a result of the generation of waves and floods in the study area in the winter of 2013

## 4. SOURCE OF THE DATA FOR MODELING (WIND FIELD DATA)

Accurate wind field data collected by meteorological models and analysis are required for excellent wave hindcasting and forecasting. Because the wind field is the primary driving factor in spectral wave models [12].

In the present work, the wind field data from (1994 - 2021) are taken from Shbicha recorded station. It's automatic weather stations belonging to the Iraqi Ministry of Agriculture that have been installed and operated near the southern Bahar AL-Najaf (Lat 31.68: log 44.3). The weather statistics show that, In the studied area, a north- northwest (NNW) wind direction predominates with a frequency of 20 %. The windiest direction over a longer period is NNW, with a Multi-year average annual maximum speed 15 (m/s). With winds gusting to 12 m/s, the N and W directions have the second-strongest winds. as seen in Figure 3. For the simulation experiments, the

least safe wind speed and direction combinations are chosen. Table 1 lists the worst-case scenario for the study area.

**Table 1.** Wind parameters in the study area for a period (1994-2021)

Location according to the Study Area	Wind Direction (Measured from True North) (Degree)	Multi-Year Average Annual Maximum Speed (m/s)
North	360	6
North – northwest (NNW)	315	15
Northwest (NW)	270	12
North(N)	0	11
Southeast(S)	135	5

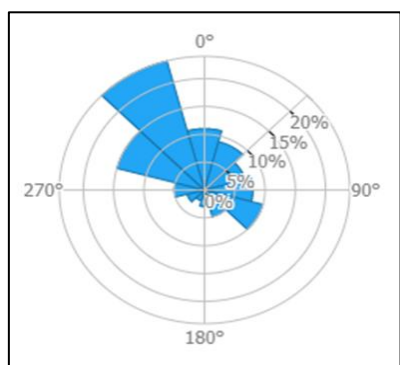


**Figure 3.** Rose chart and frequency of wind speed and direction in the project region of study area

#### 4.1 Wind speed and probability of occurrence

$P$  refers to the likelihood that an occurrence involving a random variable (such as wind speed) with magnitude equal to or higher than a specified magnitude  $X$  will occur. The recurrence interval, commonly referred to as the return time, is defined as:

$$T = \frac{1}{P} \quad (1)$$

This is the typical interval between wind events with magnitudes equal to or higher than  $X$ . The correct formula offers the probability  $P$  that an event will occur with a value of equal to or higher than.

$$P = \frac{m+0.41}{N+0.53} \quad (2)$$

After calculating  $P$  for each event in the series, the variation of the velocity wind magnitude is shown on a semi-log graph against the matching  $P$ . The velocity wind magnitude of specified height for any  $P$  may be determined using proper extrapolation of this figure within applicable constraints.

$$K = -0.7797 * \left[ 0.5772 + \ln \left( \ln \frac{T}{T-1} \right) \right] \quad (3)$$

According to the previous study, the general equation of hydrologic frequency analysis may be used to describe the bulk of frequency distribution functions relevant to hydrologic investigations.  $X_T = u + K * s$ ; where  $u$  is the mean,  $s$  is the standard deviation, and  $K$  is the frequency factor that depends

on the return period,  $T$ , and the assumed frequency distribution, and  $X_T$  is the value of the variate  $X$  in a random hydrologic series with a return time  $T$ .

$$ST = 2\sqrt{\{1 + 1.1396K + 1.1K^2\} * \frac{s^2}{N}} \quad (4)$$

Figure 4 and Table 2 displays the wind speeds for various return durations that were translated to 10 meters above sea level [13].

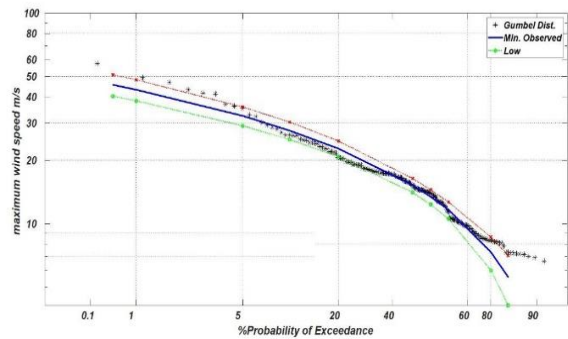


**Figure 4.** Represent maximum wind speed for different probability of exceedance

**Table 2.** Wind speeds at the Shbicha station for different return periods (unit: m/s) for maximum monthly for a period (1994-2021)

T (once in)	K	Wind Speed (m/s)
25 year	2.043	21.17
50 year	2.592	22.80
75 year	2.911	23.74
100 year	3.136	24.41
Mean speed=15.12 (m/s), Standard deviation=2.96, Coefficient of variation=0.195, Coefficient of skewness=0.3082, Alfa parameter=2.3086, Beta parameter=16.4575, Kurtosis coefficient=3.046		

#### 5. SPECTRAL WAVE MODELING (MIKE 21) DHI

Wave climates at offshore and coastal places may be estimated with the help of DHI Water and Environment's MIKE 21 SW spectral wind-wave model. It promotes the development, degradation, and modification of wind-generated waves and swells in offshore and coastal regions. Because exact wave load estimates are critical for both safety and economic reasons, it is extensively used in the construction of offshore, coastal, and portal buildings.

The three primary computational procedures for computing wave fields are the energy balance equation, the mild slope equation, and the Boussinesq equation. Because of the physical assumptions made, each approach has a limited applicability range. An effective mathematical model for describing the motion and distortion of coastal waves is the Mild slope equation. Nevertheless, it is not appropriate for complicated settings with quick topographical changes because of its challenging analytical solution, demanding processing needs, and absence of white wave loss and wind energy input.

The Boussinesq equation include that in calculation: refractions, shallow water deformations, diffractions, and reflections of waves; nevertheless, it is restricted by the depth of the water and requires a lot of labor to compute, which is

why it is only helpful for calculating wave behavior over very small regions.

The wave spectrum model MIKE21 SW, which is based on a mass conservation of wave action, can handle a variety of situations, including wind waves, nonlinear waves interactions, whitecaps loss, friction loss caused by bottom, wave breaking, and reflections and diffractions, shallow water deformations [4].

The MIKE21 SW model uses central differentiation in constrained volumes for discretization. Depending on the technical and geographic conditions, both unstructured and structured grids may be used concurrently. The model may automatically adapt its time step based on the stability situation. Several sequence explicit methods and a stepwise integral in time are used in this model to calculate wave transport. The migration equation for wave density is solved to describe the dynamic mechanics of gravity waves. Since the wave density spectrum varies with time (t) and space (x, y), it is a function of two-phase parameters. The two-phase parameters in this model are the relative wave frequency  $s$  and the wave direction (in degrees). The basic equation is as follows:

$$\frac{\partial N}{\partial t} + \nabla \cdot (\nabla N) = \frac{S}{\sigma} \quad (5)$$

where,  $S$  is the source term (J),  $t$  is time (s),  $v$  is the wave group's propagation velocity in the four-dimensional phase, and  $N$  is the energy wave (J).

### 5.1 Wave energy transient condition

When considering the link between the wave energy spectral density  $E(\sigma)$  and the wave action density  $N(\sigma)$ ,  $\partial N/\partial t$  reflects the change of wave energy with regard to time.

$$N(\sigma, \theta) = \frac{E(\sigma, \theta)}{\sigma} \quad (6)$$

The relationship between the absolute and relative wave frequencies is seen in the graph. In the discretized linear equation, their connection may be represented as follows:

$$\sigma = \sqrt{gk \tanh(kd)} = \omega - k \cdot U \quad (7)$$

where,  $L$  is the wavelength,  $k$  is the wave vector,  $k=2/L$ ,  $U$  is the flow velocity vector, and  $g$  is the acceleration of gravity.

### 5.2 Frequency and direction-domain variations in wave energy

With regard to the geo-domain, frequency domain, and direction domain, wave energy changes are represented by the  $\nabla \cdot (\nabla N)$ . The major causes of changes in the frequency domain are variations in the water depth and flow rate. The fractions caused by the water depth and flow speed are represented as changes in the direction domain:

$$v = (c_x \cdot c_y \cdot c_\sigma \cdot c_\theta) \quad (8)$$

where,  $c_*$  is the variation in the frequency caused by changes in the level of water and flow speed (Hz/s);  $c_*$  is the fraction caused by the changes in level of water and flow; and  $c_x$  and  $c_y$  are changes in the wave propagation in the  $x$  and  $y$  directions, respectively (measured in m/s).

$$c_x = \frac{dx}{dt} = \frac{1}{2} \left[ 1 + \frac{2kd}{\sin h(2kd)} \right] \cdot \frac{\sigma k_x}{k^2} + U_x \quad (9)$$

$$c_y = \frac{dy}{dt} = \frac{1}{2} \left[ 1 + \frac{2kd}{\sin h(2kd)} \right] \cdot \frac{\sigma k_y}{k^2} + U_y \quad (10)$$

$$c_\sigma = \frac{d\sigma}{dt} = \frac{\partial \sigma}{\partial d} \left( \frac{\partial d}{\partial t} + U \cdot \nabla d \right) - c_g k \cdot \frac{\partial U}{\partial s} \quad (11)$$

$$c_\theta = \frac{d\theta}{dt} = -\frac{1}{K} \left( \frac{\partial \sigma}{\partial t} \frac{\partial d}{\partial m} + k \cdot \frac{\partial U}{\partial m} \right) \quad (12)$$

where,  $s$ =direction coordinate,  $m$ =perpendicular coordinate to  $s$ ,  $U_x$  and  $U_y$  are the components of  $U$ ,  $k_x$  and  $k_y$  are the components of  $k$ ,  $c_g$  is the magnitude of the group velocity, and so on.

### 5.3 Source function

The energy conservation equation, which is shown as a spectral density, uses  $S$  as the source function. According to Water and Environment DHI (2016), it is the superposed form of the source functions of a range of physical phenomena.

$$S = S_{in} + S_{nl} + S_{ds} + S_{bot} + S_{surf} \quad (13)$$

where,  $S_{in}$  is the energy supplied by the wind (J),  $S_{nl}$  is the energy lost as a result of nonlinear wave interactions (J),  $S_{ds}$  is the energy lost as a result of whitecaps (J),  $S_{bot}$  is the energy lost as a result of bottom frictions (J), and  $S_{surf}$  is the energy lost as a result of wave breaking as a result of changes in water depth (J).

## 6. MATHEMATICAL MODEL BUILD-UP (MIKE21SW)

The following six stages (Figure 5) will commonly make up the Model Checklist when using the newest generation spectral wind-wave models in MIKE21 SW to forecast the onset, decline, and transformation of wind-generated waves and swell in offshore and coastal environments:

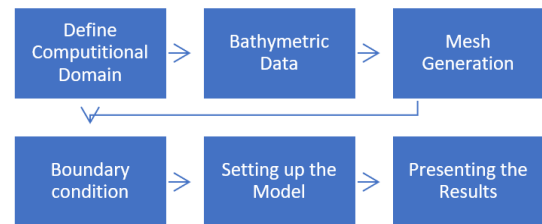


**Figure 5.** Steps of build-up MIKE21 SW model

The first step in preparing the model is to select the study area by making a shape file by uploading a high-resolution aerial image and bounded the outer boundaries of the area, then a geo-referencing of the map is made using the GIS program or any geographic information program.

The next step. Make an abstract of the downloaded bathymetry data according to the boundaries of the region in the previous step. And then we have a map that has the three coordinates XY and Z.

The next step is very important, making meshing of the area, and mark the most important zone (breakwater location) in the study by determining it with a polygon for the purpose of increasing the density of division in this zone in order to obtain

results with high accuracy. It must be ensured that the solution is no longer dependent on the values of the meshing size (mesh independent solution).

After that, the steps depend on the values of the boundary condition by determining the direction and speed of the wind and the equations that describe the spectral of the projected wind and the type of model used.

## 7. COMPUTATIONAL DOMAIN AND BATHYMETRIC DATA

The General bathymetric Chart of the Oceans and wet land (GEBCO) consists of an international group of experts in ocean mapping. This organization it is provide the most authoritative publicly available bathymetry of the world's oceans. Bathymetric data at each site, where available, was

provided in the form of hydrographic charts (Iraq, Najaf) or in digital X, Y, Z format and additional gridded data from GEBCO. Using MIKE 21 go-referencing, the hydrographic charts were digitized, and the digital data entered was transformed to MIKE21 forms. The computational grids for target area were then made utilizing these data sets and the Mesh editor in MIKE21-mesh generation (Figure 6).

The main purpose of preparing this study is how to employ energy dispersal facilities and breakwater orientations to protect the zone selected in the road of Maamal (Figure 7). Three distinct layouts with varied breakwater lengths and azimuths were considered (Figure 8 and Figure 9). The impact of the breakwater on the wave field under various circumstances was then studied in order to give the construction unit with accurate simulation results (Table 3). Figure 10 depicts the breakwater's design with various azimuths and lengths.

**Table 3.** Details of three schemes breakwater layout and results of MIKE21 SW model and points features

Breakwater Scheme	Point Monitor	x-coordinates m	y-coordinates m	Sign Wave High (m)	Covering Area with Wave Sign Height Less Than 0.7 m (km <sup>2</sup> )	Length of Shoreline Protect (Km)
Scheme 1	P <sub>1</sub>	432431.798	3538289.742	0.77	1.19 km <sup>2</sup>	1.89 km
	P <sub>2</sub>	432449.762	3538501.743	0.76		
	P <sub>3</sub>	432658.172	3538778.423	1.22		
	P <sub>4</sub>	432884.546	3539051.509	1.23		
	P <sub>5</sub>	432913.292	3539026.356	0.72		
	P <sub>6</sub>	432557.345	3538778.423	0.12		
	P <sub>7</sub>	432482.103	3538494.557	0.09		
	P <sub>8</sub>	432482.103	3538296.929	0.54		
Scheme 2	P <sub>1</sub>	432844.678	3538361.876	0.79	0.889 km <sup>2</sup>	1.65 km
	P <sub>2</sub>	432822.900	3538522.123	0.77		
	P <sub>3</sub>	433034.678	3538811.900	1.21		
	P <sub>4</sub>	433257.123	3539062.122	1.15		
	P <sub>5</sub>	433279.124	3539044.234	0.65		
	P <sub>6</sub>	433077.236	3538800.129	0.11		
	P <sub>7</sub>	433850.234	3538525.789	0.08		
	P <sub>8</sub>	432869.654	3538361.876	0.50		
Scheme 3	P <sub>1</sub>	432444.157	3538478.203	0.833	1.11 km <sup>2</sup>	1.77 km
	P <sub>2</sub>	432617.372	3538705.032	1.22		
	P <sub>3</sub>	432800.898	3538940.110	1.23		
	P <sub>4</sub>	432969.989	3539164.877	0.78		
	P <sub>5</sub>	433000.009	3539137.213	0.253		
	P <sub>6</sub>	432851.053	3538934.092	0.148		
	P <sub>7</sub>	432661.473	3538685.832	0.168		
	P <sub>8</sub>	432489.949	3538464.655	0.54		

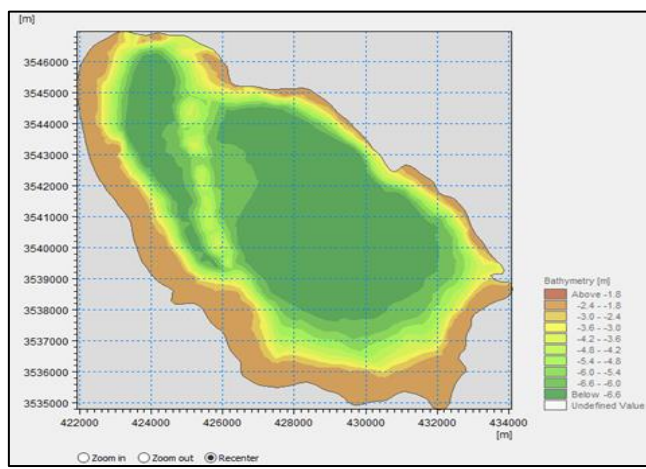


**Figure 6.** Bathymetry map (x, y, and z)



**Figure 7.** Image in survey region (Proposed Breakwater)

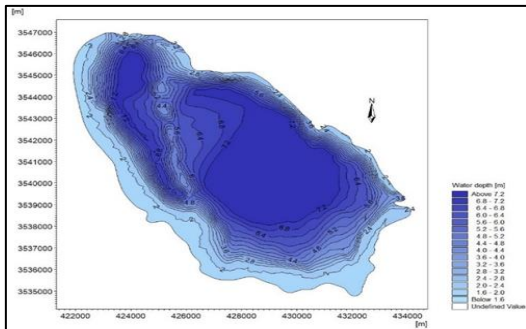


**Figure 8.** Water depth according to bathymetry data

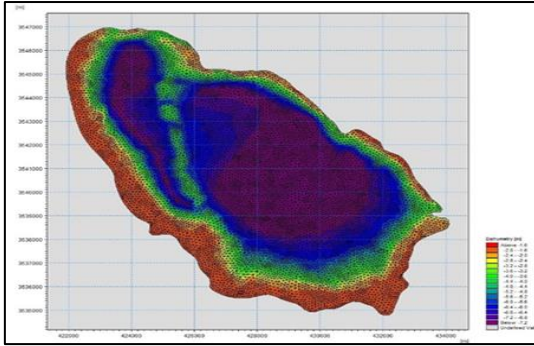


**Figure 9.** Mesh discretization for domain

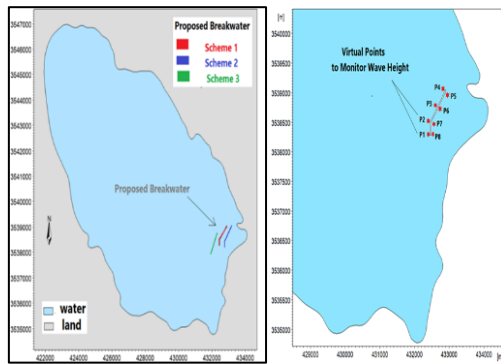


**Figure 10.** Layout of proposed breakwater and virtual points to monitor wave high inside and lee side breakwater

**Table 4.** Result of average wave height for empirical formula and numerical model

Calculation Position	Water Depth H <sub>m</sub> (m)	Wind Direction	Wind Speed W (m/s)	Fetch Length (m)	h <sub>m</sub> Empirical	h <sub>m</sub> Numerical	h <sub>m</sub> Empirical-h <sub>m</sub> Numerical
O1	5.10	NNW (360°)	9	11345	0.89	1.01	0.12
O2	5.60	NW (315°)	15	12678	1.25	1.31	0.06
O3	4.75	NNW (290°)	12	11690	1.21	1.29	0.08
O4	4.11	NNW (270°)	7	7689	0.76	0.73	0.03
O5	4.67	NNW (260°)	5	6567	0.52	0.5	0.02

## 9. LAYOUT OF BREAKWATER SPECIFICATION

Table 5 below described the three-scheme layout for breakwater specification in the different orientation and direction. Figure 12 shows the Significant wave height distribution in the direction NNW (315°) for three different Scheme, it is clear from these figures that the scheme 1 scenario of the breaker layout gives the highest efficiency to reduce the wave level in the concerned area and covers the highest area on the coast and the adjacent area of wave activity.

Table 5, Figure 12 demonstrates the change in wave height

## 8. MATHEMATICAL MODEL ESTABLISHMENT AND VALIDATION

In clearly, the validation of a mathematical model (MIKE21SW) involves comparing its predictions with actual observations, measurements to ensure its accuracy and reliability for real-world applications.

Three of the most often utilized empirical equations in the field of wave high and period measurements are the Guanting formula, the Hedi formula, and the Putian formula. In accordance with studies by Li et al. [14] and Zheng et al. [15], the Putian formula may be used to determine the average height and period of water waves. the Putian formula was proposed by Duan et al. [16] to calculate wave run-up height according to six years of observation at the seawall of Putian, China. In 2002, and gave good results as mentioned in many studies as mentioned above.

$$\frac{gh_m}{w^2} = 0.13 \tanh \left[ 0.7 \left( \frac{gH_m}{w^2} \right)^{0.7} \right] \tanh \left\{ \frac{0.0018 \left( \frac{gD}{w^2} \right)^{0.45}}{0.13 \tanh \left[ 0.7 \left( \frac{gH_m}{w^2} \right)^{0.7} \right]} \right\} \quad (14)$$

where,  $D$  is the length of the wind zone or fetch (m),  $H_m$  is the average sea depth (m),  $h_m$  is the average wave height (m),  $t_m$  is the average wave period (s), and  $w$  is the computed wind speed (m/s).

To confirm the reliability of the MIKE21 SW model, the wave heights are calculated for the case study under natural conditions using the model and the empirical formula. The empirical formula results compared to the SW model are shown in Table 4 and Figure 11.

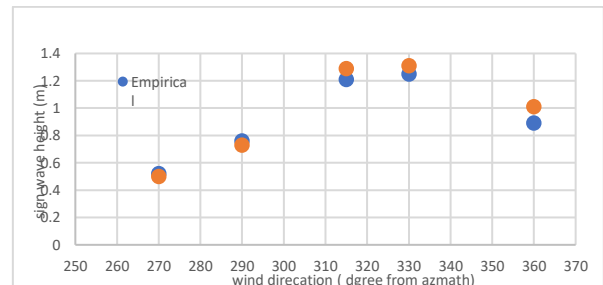


**Figure 11.** Comparison between empirical and numerical results

and the direction of the waves both before and after the construction of the breakwater. The wave heights at the upstream and downstream were measured after the breakwater had been constructed, and they were found to be between 0.35 and 0.7 m (Figure 13). This implies a decrease of around 40% to 60% in comparison to the original heights of 1.25 to 0.9 m. Figure 6 shows the Significant wave height distribution for many wind directions expected, it is clear that from these figures the position of maximum wave high is variation according to the wind direction [17, 18].

**Table 5.** Layout of breakwater

Scheme Proposed	Details of Mitigations Structure
<b>Scheme 1</b>	The breakwater is 800 meters long in total; the broken line sections on the south and east sides are each 170 meters long. Crest level = mean sea level MSL
<b>Scheme 2</b>	The breakwater is 862 meters long overall; the sections with broken lines on the west and east sides are each 177 meters long. Crest level = mean sea level MSL
<b>Scheme 3</b>	The breakwater is 879 metres long and is oriented in a straight line at a 36-degree angle from the azimuth. Crest level = mean sea level MSL

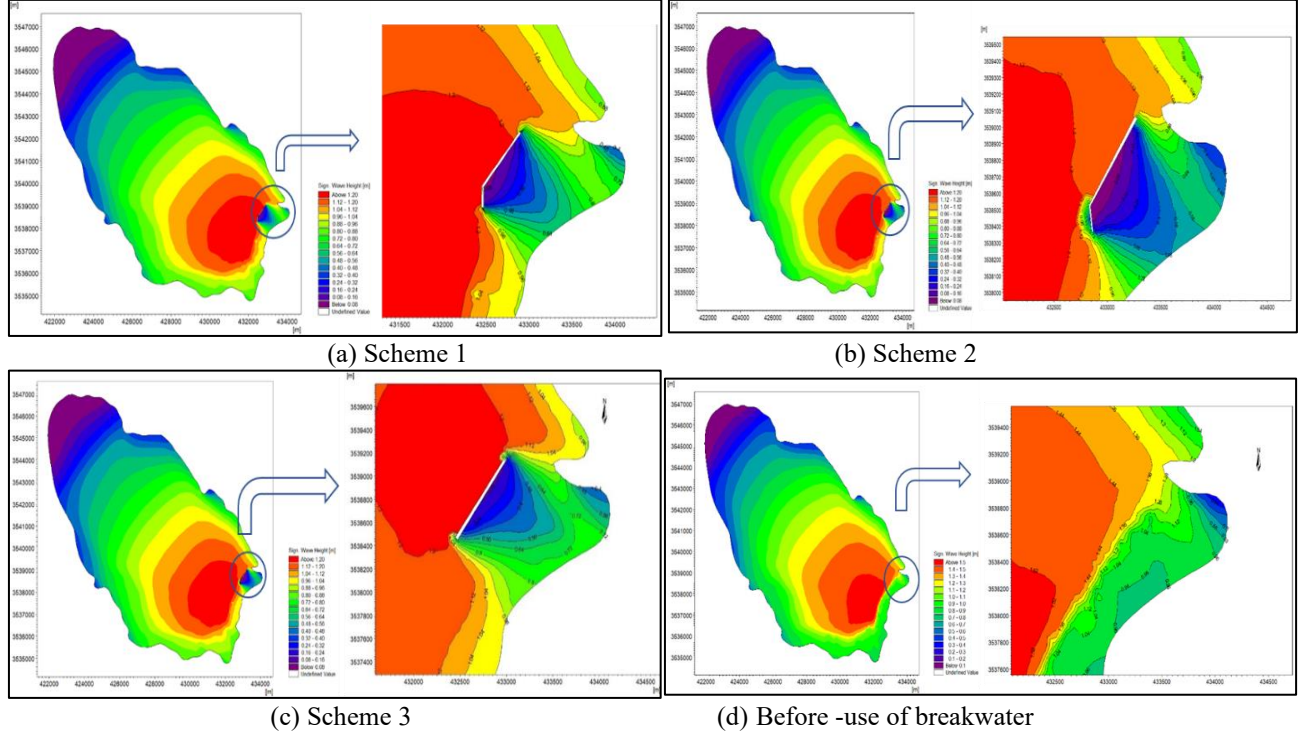


**Figure 12.** The Significant wave height distribution in the direction NNW (315°) for three different Scheme

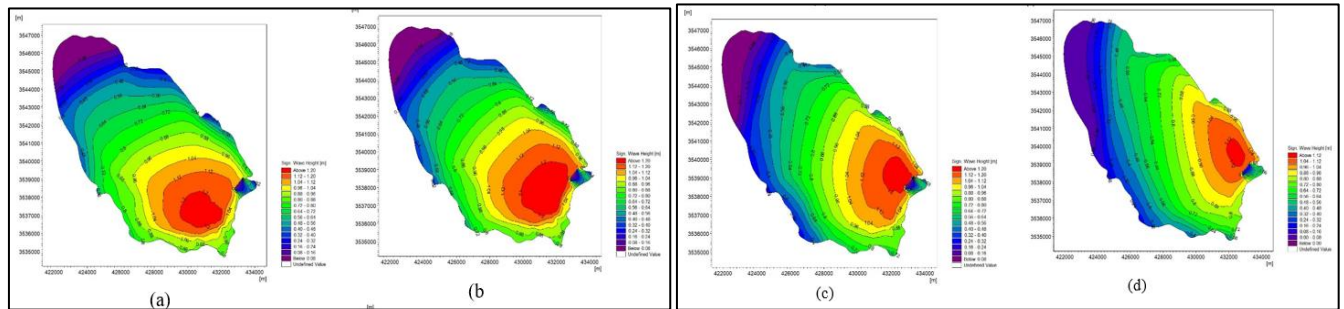


**Figure 13.** The significant wave height distribution for many wind directions expected (a) NNW 330°, (b) NNW 315°, (c) NW 290 and (d) WW 270°

## 10. DISCUSSION AND CONCLUSIONS

Given the limited amount of knowledge on numerical modelling of the wave field in lake or shallow reservoirs, the current study was conducted on plain shallow water depression of Najaf sea using the MIKE21 SW model.

The amount of variation between the simulated wave heights and those calculated using an empirical equation is less than 9%. As a result, the MIKE21 SW model can simulate wind-generated waves in simple shallow water lakes.

In the simulation, a number of breakwaters with a variety of settings for their orientation and placement were used. The results showed that the three schemes used for the breakwater

gave varying results, both depending on its location and characteristics. The first scheme gave a covering area approaching 1.19 km<sup>2</sup>, and the second scheme gave approximately 0.889 km, and third scheme gave a covering area 1.11 km<sup>2</sup>. The results of scheme 1 Figure 11 indicated that it was the most successful at reducing the wave height and covered the most area (1.19 km<sup>2</sup>) along the coast line of the target region. The findings make it abundantly evident that waves breaking close to shore are greatly influenced by bathymetric data. This highlights how important it is to have good bathymetric measurements of the waters near the beach. In summary, As can be seen from the wave field distribution and the variation of wave parameters at the feature points, if

the proposed project is implemented, wave height behind the breakwater would be significantly lower than it was before the project, and Scheme 1 would have a better improvement effect on wave conditions.

## REFERENCES

- [1] Dean, R.G., Dalrymple, R.A. (1991). Water wave mechanics for engineers and scientists (Vol. 2). World Scientific Publishing Company. <https://doi.org/10.1142/1232>
- [2] Zhang, W. (2013). Study on the suspension flux of substance in nearshore and its application in Jiangsu sea area. Ph.D. Thesis, Hohai University, Nanjing, China.
- [3] Wang, S.P., Li, R.J., Ming, J.I., Dong, X.T., Zhu, W.J. (2015). Combined application of swan and cgwave model in calculation of design wave parameters. *J. Waterw. Harb.*, 4: 308-312.
- [4] DHI, M. (2017). MIKE 21 Spectral Wave Module, Scientific Documentation. Hørsholm, Denmark: DHI Water Environment Health.
- [5] Li, Y., Huang, Z., Zhang, J.F., Wu, W.J., Zhang, C.F., Zhao, Q.F. (2014). Application and verification of sea wave forecast by WAVEWATCH III model in the Bo hai Sea of China. *Journal of Meteorology and Environment*, 30(1): 23-29. <https://doi.org/10.3969/j.issn.1673-503X.2014.01.004>
- [6] Bi, F., Song, J., Wu, K., Xu, Y. (2015). Evaluation of the simulation capability of the Wavewatch III model for Pacific Ocean wave. *Acta Oceanologica Sinica*, 34: 43-57. <https://doi.org/10.1007/s13131-015-0737-1>
- [7] Yang, X.C., Zhang, Q.H. (2013). Joint probability distribution of winds and waves from wave simulation of 20 years (1989-2008) in Bohai Bay. *Water Science and Engineering*, 6(3): 296-307.
- [8] Ayat, B. (2013). Wave power atlas of eastern mediterranean and aegean seas. *Energy*, 54: 251-262. <https://doi.org/10.1016/j.energy.2013.02.060>
- [9] Noujas, V., Thomas, K.V., Ajeesh, N.R. (2017). Shoreline management plan for a protected but eroding coast along the southwest coast of India. *International Journal of Sediment Research*, 32(4): 495-505. <https://doi.org/10.1016/j.ijsrc.2017.02.004>
- [10] Omran, H.A., Mahmood, M.S., Abbas, A. (2014). Quantity and distribution of the current surface and ground water resources in bahr an-najaf in Iraq.
- [11] Farhan, A.A., Abed, B.S. (2021). Estimation of surface runoff to Bahr Al-Najaf. *Journal of Engineering*, 27(9): 51–63. <https://doi.org/10.31026/j.eng.2021.09.05>
- [12] Xiang, Y., Fu, Z.M., Meng, Y., Zhang, K., Cheng, Z.F. (2019). Analysis of wave clipping effects of plain reservoir artificial islands based on MIKE21 SW model. *Water Science and Engineering*, 12(3): 179-187. <https://doi.org/10.1016/j.wse.2019.08.002>
- [13] Chanson, H. (2004). *Hydraulics of open channel flow*. Elsevier.
- [14] Li, J.F., Qi, Y.X., Sun, J. (2006). The primary discussion on calculation method of reservoir crest super elevation in the plain area. *J. Northwest Hydroelectric Power* 22(5): 41e43.
- [15] Zheng, D.X., Zhou, R.X., Jin, R.Q., Zheng, L. (2009). Discussion on the calculation method of plain reservoir wave run-up. *Yellow River*, 3: 86-87.
- [16] Duan, X., Mao, P., Mao, C. (1996). Research on the status of seawall along the southeast coast (Fujian Province). *Ocean Eng.*, 14: 41–49. <https://doi.org/10.3390/jmse10121809>
- [17] [http://www.gebco.net/data\\_and\\_products/gridded\\_bathymetry\\_data/](http://www.gebco.net/data_and_products/gridded_bathymetry_data/).
- [18] <https://apps.sentinel-hub.com/eo-browser>.